DR-1829-5

UCLA

UCLA-ENG-8611
PPG-937

Materials Data Base and Design Equations For the UCLA Solid Breeder Blanket

Shahram Sharafat, Robert Amodeo and Nasr M. Ghoniem

February 1986

FUSION PHYSICS & ENGINEERING

MECHANICAL, AEROSPACE AND NUCLEAR ENGINEERING DEPT.
AND
CENTER FOR PLASMA PHYSICS AND FUSION ENGINEERING
UNIVERSITY OF CALIFORNIA, LOS ANGELES

UCLA-ENG--8611

DE86 012971

UCLA-ENG-8611
PPG-937

Materials Data Base and Design Equations For the UCLA Solid Breeder Blanket

Shahram Sharafat, Robert Amodeo and Nasr M. Ghoniem

February 1986

This work was supported by the U.S. Department of Energy, Office of Fusion Energy, Grant #DE-[redacted]03-80ER52061, with UCLA.

AS

DISCLAIMER

EBB

TABLE OF CONTENTS

FIGURES

TABLES

MATERIALS DATA BASE AND DESIGN EQUATIONS

I. Introduction

The need for a complete and coherent material data base for fusion reactor systems has been an important issue for some time now. Since the choices for materials used in fusion reactors are becoming more apparent, it is important to be able to quickly access this data to facilitate reactor design. The problem with the current choices of materials is that there is not enough data available to supply complete information on all the important material properties under anticipated fusion operating conditions. In places where there is a deficit in data, it is therefore necessary to extrapolate information to support analysis which covers ranges of undetermined values.

The philosophy of a data base is one of expansion and modification. This will lead to a constantly growing collection of most recently acquired information. Based on this philosophy special care has been given to the structure, the accessability and ease of modification. The data base is developed primarily for use on Personal Computers (PC s). The PC enhances accessability due to their widespread use. The final version of the data base will have the format of a tree-structure, which will allow the user to access the information in form of raw data, plots or equations. In many instances the equations are not simple fits to the data but we have developed phenomenological equations based on analytical interpretations.

In section 2 we will list materials and properties investigated for this blanket study. Section 3 is a list of phenomenological equations and mathematical fits for all materials and properties considered. Section 4 describes our efforts to develop a swelling equation based on the few

experimental data points available for breeder materials. In section 5 we investigate the sintering phenomena for ceramics.

2. Material Properties

The present reactor study investigated the following materials as candidates for the Fusion Power Core (FPC): ferritic steels HT-9, and 2 1/4 Cr-1 Mo, blanket breeder ceramics $LiAlO_2$ and Li_2O; and blanket neutron multiplier material beryllium. Li_2O was ruled out as a candidate for solid breeder material due to its high anticipated swelling behavior. Nevertheless we will discuss some of our findings about Li_2O in Section 4.

The data on all materials was compiled form various sources, mainly the Materials Handbook for Fusion Energy Systems [1], and recent experimental investigation by Hollenberg [2] and Rasneur [3]. The Materials Handbook includes a comprehensive work on the ferritic steel 2 1/4 Cr - 1 Mo, of which much information has been determined over the last decade. Mechanical properties data and thermal data most relevant reactor blanket designs are listed in Table 1. Some of the data on the ferritic steel HT-9 is also derived from the Materials handbook. Most of the data used for this report, however, comes directly from the Sandvik Steel Co. reports on HT-9 mechanical properties [4].

Other data on the ferritic steels include steady state thermal creep correlations [5]. The expression used for swelling of the ferritic steel 2 1/4 Cr - 1 Mo is from work by Gelles and Puigh [6] on irradiation induced swelling. Since observed swelling is a bilinear phenomenon, this fit to the data produces a smooth transition from one swelling rate to another at the critical value of dose. The expression used for the ferritic steel HT-9

is based on a fit from work by Ghoniem [7]. It does not produce a smooth transition, and therefore the value of swelling should be set to zero below the incubation dose. The correlation used for irradiation creep of HT-9 is also based on an expression previously developed for 2 1/4 Cr - 1 Mo [6].

Information on material properties of lithium aluminate and lithium oxide is derived chiefly from Hollenberg [2] and Rasneur's work [3]. Some of the data displayed in this paper is in raw format, and requires transforming into suitable units for proper use. In addition, much of the information was sparse and scattered, and extrapolation techniques were used to fill in the data. In particular, the phenomenon of swelling and process of sintering of these breeder ceramics have not been measured in much detail. However, correlations were developed from these data and are discussed in section 3.

In order to determine the tritium breeding behavior of $LiAlO_2$, Rasneur [3] examined properties of very homogeneous microtextures of porous $LiAlO_2$ in an in-situ tritium extraction experiment. From a large field of homogeneous microstructures, empirical equations were deduced as a function of porosity, grain diameter and temperature. Mechanical and thermal properties examined include: ultra sound velocity, Young's modulus, ultimate compressive strength, creep and thermal shock. Physico-chemical properties such as electrical resistivity and sensitivity to air were also investigated. Raseneur found porous $LiAlO_2$ to be an insulator even up to 600°C. Exposed to air, $LiAlO_2$ will react with H_2O vapor to form LiOH molecules. LiOH will then react with CO_2 to form Li_2CO_3 compounds. Raseneur's experiments showed that porous lithium aluminate exposed to air will have about 10 monolayers corroded after one year, i.e. less than 1% for an average grain size of 0.4μm in diameter. In water however, the reaction on identical samples was total after about only three months.

3. Phenomenological and Empirical Equations.

This section lists the data base equations which are the results of our phenomenological investigations and purely empirical fits performed by us or by mentioned authors.

We start with ferritic steels HT-9 and 2 1/4 Cr - 1 Mo and conclude this collection with breeder material properties listed in Table 1.

TABLE 1

Summary for Blanket Material Properties
Current Status (12/85)

Ferritics	
HT-9	2 1/4 Cr - 1 Mo
Young's Modulus	Young's Modulus
Shear Modulus	Shear Modulus
Poisson's Ratio	Poisson's Ratio
Ultimate Tensile Strength	Ultimate Tensile Strength
Instantaneous Thermal Expansion	Thermal Expansion
Mean Thermal Expansion	Thermal Conductivity
Linear Thermal Expansion	Void Swelling
Steady State Thermal Creep	Steady State Thermal Creep
Irradiation Creep	Irradiation Creep

Breeder	
Lithium Oxide	Lithium Aluminate
Young's Modulus	Young's Modulus
Shear Modulus	Shear Modulus
Poisson's Ratio	Poisson's Ratio
Sintered-Thermal Conductivity	Sintered Thermal Conductivity
Sphere Packed-Thermal Conductivity	Sphere Packed-Thermal Conductivity
Creep Rate	Creep Rate
Thermal Expansion	Thermal Expansion
Specific Heat	Specific Heat
Fission Gas Swelling	Fission Gas Swelling
Fracture Strength	Ultra Sound Velocity
	Ultimate Compressive Strength

* Only the fission gas (Helium) swelling behavior of Beryllium was investigated.

3.1 FERRITIC STEELS

1. HT-9

Young's Modulus YM (T °F) MPa

$$YM = (A_1 + A_2T + A_3T^2) \times 10^3$$

Poisson's Ratio PR (T °F)

$$PR = B_1 + B_2T + B_3T^2$$

Shear Modulus SM (T °F) MPa

$$SM = YM/2(1 + PR)$$

Ultimate Tensile Strength [8] UTS (T K) MPa

$$473 < T < 873$$

$$UTS = C_1 + C_2T + C_3T^2 + C_4T^3$$

Instantaneous Thermal Expansion Coefficient ITE (T °C) $10^{-6}/°C$

$$21 < T < 650$$

$$ITE = D_1 + D_2T + D_3T^2$$

Mean Thermal Expansion Coefficient MTE (T °C) $10^{-6}/°C$

$$37 < T < 650$$

$$MTE = (E_1 + E_2T + E_3T^2 + E_4T^3)/(T - 25)$$

Linear Thermal Expansion LTE (T ^{o}C) mm/m

$$21 < T < 650$$

$$LTE = F_1 + F_2T + F_3T^2 + F_4T^3$$

Steady State Thermal Creep Rate [8] TCR (σ ksi, T K) s^{-1}

$$TCR = (B'/kT)(\sigma - \sigma_{1_o})^3 \, e^{(-Q1/kT)}$$

$$B' = 7.385 \times 10^{-3}$$

$$\sigma_{1_o} = aT + C \quad \text{ksi}$$

$$a = -.2185 \text{ ksi/K}$$

$$C = 198.1783$$

$$Q1 = 1.23 \text{ eV}$$

Irradiation Creep [9] IC (σ_{eff} ksi, Φ n/cm^2-s, t s) %

$$IC = K' \, \sigma_{eff}^{1.5} \, \Phi \, t$$

$$K' = 0.4 \times 10^{-4} \text{ (MPa)}^{-1} \text{ } (10^{22} \text{ n/cm}^2) \text{ (\%)}$$

Void Swelling [8] VS (δ DPA, T °C) %

$$VS = C'(\delta - \delta_o) \, e^{-((T - 425)/59)^2}$$

$$C' = 0.025 \quad \% \text{ / DPA}$$

$$\delta_o = 90 \text{ DPA}$$

2. 2 1/4 Cr - 1 Mo

Young's Modulus YM (T °F) MPa

$$YM = (G_1 + G_2T + G_3T^2 + G_4T^3) \times G_5$$

Poisson's Ratio PR (T °F)

$$PR = H_1 + H_2T + H_3T^2$$

Shear Modulus SM (T °F) MPa

$$SM = YM/2(1 + PR)$$

Ultimate Tensile Strength [8] UTS (T K) MPa

$$473 < T < 873$$

$$UTS = I_1 + I_2T + I_3T^2 + I_4T^3$$

Thermal Expansion Coefficient TE (T °C) 10^{-6}/°C

$$20 < T < 700$$

$$TE = J_1 + J_2T + J_3T^2$$

Thermal Conductivity TC (T °C) W/cm-K

$$25 < T < 700$$

$$TC = K_1 + K_2T + K_3/T + K_4T^2$$

Steady State Thermal Creep Rate[8] TCR (σ ksi, T K) s^{-1}

$$TCR = (A'/kT)(\sigma - \sigma_{2_o})^4 \, e^{(-Q2/kT)}$$

$$\ln A' = 17.2898$$

$$\sigma_{2_o} = aT + C$$

$$a = -0.0628$$

$$C = 51.7929$$

$$Q2 = 2.767 \text{ eV}$$

Irradiation Creep [9] IC (σ_{eff} ksi, Φ n/cm^2-s, t s) %

$$IC = K' \sigma_{eff}^{1.5} \Phi t + D S \sigma_{eff}$$

$K' = 0.4 \times 10^{-4}$ (MPa)$^{-1}$ (10^{22} n/cm^2) (%)

D = swelling enhanced creep coefficient

$= 2.7 \times 10^{-5}$ (MPa)$^{-1}$ (10^{22} n/cm^2)

S = fractional swelling rate (% / 10^{22} n/cm^2)

Void Swelling [9] VS (Φ n/cm^2, t s) %

$$VS = VS_1 - D$$

$$VS_1 = R \left[\Phi t + \frac{1}{\alpha} \ln \left[\frac{1 - \exp(\alpha(\gamma - \Phi t))}{1 + \exp(\alpha t)} \right] \right]$$

D = Densification Term

$= D(1 - e^{(-\lambda \Phi t)})$

D = steady state density (= -0.08%)

λ = transition parameter (= 3 (10^{22} n/cm^2))

γ = swelling incubation parameter

= $C_1 \exp(C_2(T - C_3)^2)$

C_1 = transition parameter

C_2 = 2.0 x 10^{23} n/cm^2

C_3 = 5.0 x 10^{-5} (K)$^{-2}$

α = swelling rate (= 0.5 (10^{22} n.cm^2)$^{-1}$)

R = 0.25% / 10^{22} n/cm^2

Table of Constants for Ferritic Steel Equations

1. HT-9

A1 : 213.28	B1 : 0.2762
A2 : -4.799×10^{-2}	B2 : 8.9309×10^{-5}
A3 : -4.065×10^{-6}	B3 : -6.262×10^{-8}

C1 : 299.7298	D1 : 9.2207
C2 : -1.11815	D2 : 1.5161×10^{-2}
C3 : 1.98127×10^{-3}	D3 : -1.0624×10^{-5}
C4 : -1.179135×10^{-6}	

E1 = -235.2	F1 : -.23520
E2 = 9.2207	F2 : 9.2207×10^{-3}
E3 = 7.5806×10^{-3}	F3 : 7.5806×10^{-6}
E4 = -3.5412×10^{-6}	F4 : -3.5412×10^{-9}

2. 2 1/4 Cr - 1 Mo

$G1 = 31.1$

$G2 = -1.359 \times 10^{-2}$

$G3 = 2.505 \times 10^{-5}$

$G4 = -2.007 \times 10^{-8}$

$G5 = 6.89475 \times 10^{3}$

$H1 = 0.254$

$H2 = 1.54 \times 10^{-4}$

$H3 = -1.26 \times 10^{-7}$

$I1 = 152.7886$

$I2 = -0.5938$

$I3 = 1.43787 \times 10^{-3}$

$I4 = -1.060566 \times 10^{-6}$

$J1 = 11.281$

$J2 = 6.97817 \times 10^{-3}$

$J3 = -3.8036 \times 10^{-6}$

$K1 = 0.64986$

$K2 = -0.2784 \times 10^{-3}$

$K3 = -82.462$

$K4 = 6407.375$

3.2 BREEDER CERAMICS

I. Lithium Oxide (Li_2O)

T_m = 1433 °C

ρ_{Li} = 0.93 g/cm^3

k = 3.4 W/mK

Notations are as follow:

T = temperature

T_m = melting point temperature

ρ = density

P = porosity

1) YOUNG'S MODULES (E)

$$E = 140 \exp(-4P)[(1-T)\exp(1-T_m/T)] \text{ GPa}$$

2) POISSON'S RATIO (η)

η = 0.25

3) SHEAR MODULUS (G)

$$G = \frac{E}{2(1+\eta)} \quad \text{(GPa)}$$

4) THERMAL EXPANSION COEFFICIENT (α)

$\alpha = a + 1.72 \times 10^{-2} T$

a = 16.05 for T in °K

a = 20.75 for T in °C

5) FRACTURE STRENGTH (σ_f)

$\sigma_f = \sigma_o[1\text{-}44\exp(-7000/T)]$ (MPa)

$\sigma_o = 108\ d^{-0.4}\ \exp(-10P)$ (MPa)

d = grain diameter

T = in °K

6) THERMAL CONDUCTIVITY (k)

SPHERE PACKED (≈ 87% SPF)

$400° \leq T \leq 1100$ °K

A) Unirradiated

(i) Helium fill-gas pressure = 6 atm.

$k = 14.220 - 2.076\ln(T) + 0.0506(\ln T)^2$ W/mK

(ii) Helium fill-gas pressure = 2 atm.

$k = 21.683 - 4.669\ln(T) + 0.259\ (\ln T)^2$ W/mK

(iii) Helium fill-gas pressure = 1 atm.

$k = 15.594 - 3.295\ln(T) + 0.182\ (\ln T)^2$ W/mK

B) Irradiated ($\Phi t > 0.5 - 2 \times 10^{26}$ n/m^2)

i) Helium fill-gas pressure = 6 atm.

$k = -0.612 + 1.679\ln(T) - 0.1905(\ln T)^2$ W/mK

ii) Helium fill-gas pressure = 2 atm.

$k = 8.937 - 1.339\ln(T) + 0.00387(\ln T)^2$ W/mK

iii) Helium fill-gas pressure = 1 atm.

$k = 16.035 - 3.681\ln(T) + 0.223(\ln T)^2$ W/mK

SINTERED

$400° \leq T \leq 1100°K$

A) Unirradiated

i) TD = 100%

$k = 42.011 - 5.407\ln(T)$ W/mK

ii) TD = 84%

$k = 72.404 - 16.146\ln(T) + 0.899(\ln T)^2$ W/mK

iii) TD = 70%

$k = 49.701 - 11.724\ln(T) + 0.708(\ln T)^2$ W/mK

B) Irradiated ($\Phi t > 0.5 - 2 \times 10^{26}$ n/m^2)

i) TD = 85%

$k = 45.602 - 11.532\ln(T) + 0.76(\ln T)^2$ W/mK

ii) TD = 70%

$$k = 29.353 - 7.751\ln(T) + 0.545(\ln T) \quad W/mK$$

7) CREEP RATE

$$\epsilon = A\sigma\exp(-E_c/kT) \quad (hr^{-1})$$

It is assumed that Li_2O will follow approximately the creep rate of UO_2. Constants for the creep equations have been correlated using melting point temperatures.

$A = 140$

$\sigma = 1.49 \times 10^4 \ (kN/m^2)$

$E_c = 2.03 \ (eV)$

for $570° \leq T \leq 900°C$

8) SPECIFIC HEAT (cp)

$$\alpha = A_1 + A_2T + A_3/T^2 \quad J/kgK$$

$A_1 = 2.5179 \times 10^3$

$A_2 = 0.3328$

$A_3 = 8.382 \times 10^{-7}$

for $306 \leq T \leq 1073 \ °K$

9) SWELLING ($\Delta V/V$)

$$\frac{\Delta V}{V} = 8.87 \times 10^{-30} \left[\frac{TfGt}{N^{1/3}} \right]^{3/2} \quad (\%)$$

f = fraction of Helium retained

G = Helium production rate ($cm^{-3}sec^{-1}$)

t = time (sec)

N = Bubble number density (cmn^{-3})

II. Lithium Aluminate

T_m = 1610 °C

ρ_{Li} = 0.28 g/cm^3

k = 1.6 W/mK

1) ULTRA SOUND (1MHz) VELOCITY (c)

$$c = c_o(1 - \frac{P}{0.7}) \quad (km^{-3}$$

where: c_o = 8.4 kms^{-1}

P = Porosity

Temperature dependence:

c is slowly decreasing by 3 to 4% form t = 25°C to 700°C.

2) YOUNG'S MODULUS (E)

$$E = \rho c^2$$

where ρ = apparent density
c = ultra sound velocity

$$E = E_o\ (1-P)\ (1-\frac{P}{0.7})^2 \quad (GPa)$$

where $E_o = \rho_o c_o^2$ (GPa)

for ρ_o = 2.615 g/cm^3

$$E_o = 184.5 \quad (GPa)$$

$$E = 184.5(1-P)(1-\frac{P}{0.7})^2 \quad (GPa)$$

3) POISSON'S RATIO

$$\eta = \eta_o/(1+0.1P)$$

$$\eta_o = 0.25$$

4) ULTIMATE COMPRESSIVE STRENGTH U.C.S.

$$U.C.S = \frac{21\exp(-10P)1}{\sqrt{d}} \quad (GPa)$$

where: d = diameter of $LiAlO_2$ grain (in microns)

For: $d = 0.42\ \mu$
$P = 0.25$

the temperature (°K) dependence was found to be

$$U.C.S. = \frac{\exp(-10P)}{\sqrt{d}} \ln\left[\frac{2200}{T}\right] \quad (GPa)$$

valid for 293° < T < 1273 °K

5) THERMAL CREEP

Creep experiments were carried out at 700°C under three loads 50, 80 and 100 MPa or samples with 0.25 porosity and 0.42 μ grain diameter.

i) Under 100 MPa

$$\frac{\Delta L}{L} = -0.0135 \ln\frac{t}{72} \qquad 200 < t < 1000 \text{ h}$$

ii) Under 80 MPa

$$\frac{\Delta L}{L} = -0.0045 \ln\frac{t}{29} \qquad 300 < t < 2000 \text{ h}$$

iii) Under 50 MPa

$$\frac{\Delta L}{L} = -0.00143 \ln\frac{t}{150} \qquad 300 < t < 2000 \text{ h}$$

Extrapolation of (iii) to 20 years leads to a creep of 1% at 700°C.

6) THERMAL CONDUCTIVITY (k)

SPHERE PACKED (≃ 87% SPF)

$500°K \leq T \leq 1200°K$

A) Unirradiated

i) Helium fill-gas pressure = 6 atm.

$$k = 25.670 - 5.5181\ln(T) + 0.297(\ln T)^2 \quad (W/mK)$$

ii) Helium fill-gas pressure = 2 atm.

$$k = 8.806 - 1.075\ln(T) \quad (W/mK)$$

iii) Helium fill-gas pressure = 1 atm.

$$k = 6.897 - 0.827\ln(T) \quad (W/mK)$$

B) Irradiated ($\Phi t > 0.5 - 2 \times 10^{26}$ n/m^2)

i) Helium fill-gas pressure = 6 atm.

$k = 8.385 - 0.999\ln(T)$ (W/mK)

ii) Helium fill-gas pressure = 2 atm.

$k = 6.823 - 0.803\ln(T)$ (W/mK)

iii) Helium fill-gas pressure = 1 atm.

$k = 5.387 - 0.619\ln(T)$ (W/mK)

SINTERED

$500° \leq T \leq 1200°k$

A) Unirradiated

i) TD = 100%

$k = 21.01 - 2.65\ln(T)$ (W/mK)

ii) TD = 84%

$k = 14.43 - 1.81\ln(T)$ (W/mK)

iii) TD = 70%

$$k = 983 - 1.221\ln(T) \quad (W/mK)$$

B) Irradiated ($\Phi t \geq 0.5 - 2 \times 10^{26}$)

i) TD = 84%

$$k = 11.097 - 1.373\ln(T) \quad (W/mK)$$

ii) TD = 70%

$$k = 6.45 - 0.771\ln(T) \quad (W/mK)$$

6) SPECIFIC HEAT (c_p)

The following measurements are available for a porosity of 0.22 and d = 0.43 μ grain diameter

Temperature (°C)	C_p (cal/g°C)
400	0.330
500	0.348
600	0.365

7) LINEAR EXPANSION FACTOR ($\Delta L/L$)

(Tn °C)

$$\frac{\Delta L}{L} = 7.43 - 2.95\ln(T) + 0.295(\ln T)^2 \quad (\%)$$

8) SWELLING ($\Delta V/V$)

$$\frac{\Delta V}{V} = 8.87 \times 10^{-30} \left[\frac{TfGt}{N^{1/3}} \right]^{3/2}$$

where: T = temperature (°K)

G = Helium production rate ($cm^{-3}sec^{-1}$)

N = Bubble number density (cm^{-3})

f = Fraction of helium retained

3.3 Selected Plots for the following Material Properties

HT-9 and 2 1/4 Cr - 1 Mo:

Young's Modulus

Shear Modulus

Poisson's Ratio

Ultimate Tensile Strength

Li_2O and $LiAlO_2$:

Thermal Conductivity

Sintered Irradiated 84%, 70% TD

Sintered Unirradiated 100%, 84%, 70% TD

Thermal Expansion Coefficient

Specific Heat

Creep Rate

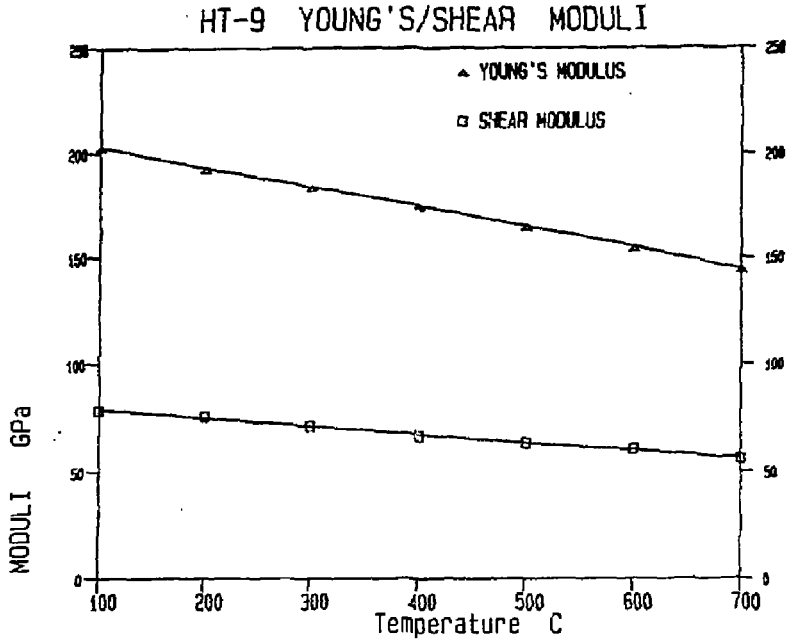
HT-9 YOUNG'S/SHEAR MODULI
YOUNG'S MODULUS
SHEAR MODULUS
MODULI GPa
250
200
150
100
50
0
100
200
300
400
500
600
700
Temperature C

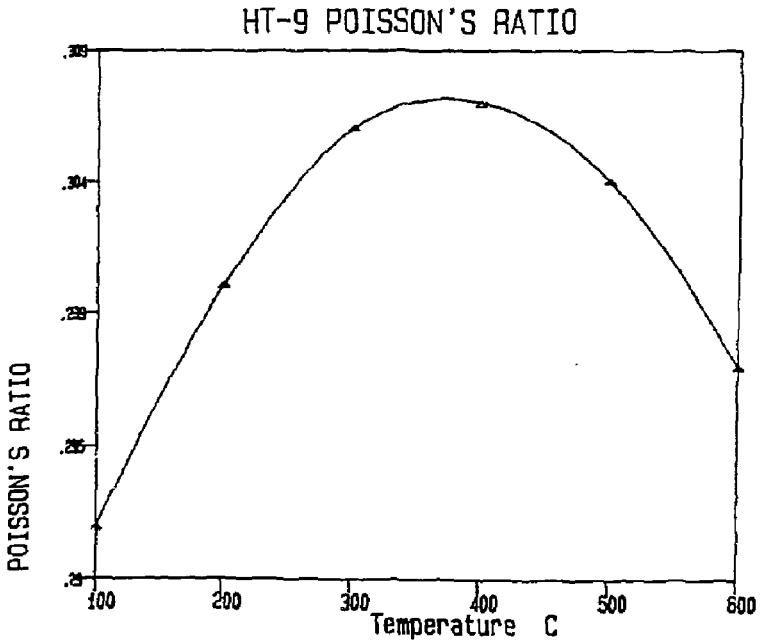
HT-9 POISSON'S RATIO
POISSON'S RATIO
.304
.285
100
200
300
400
500
600
Temperature C

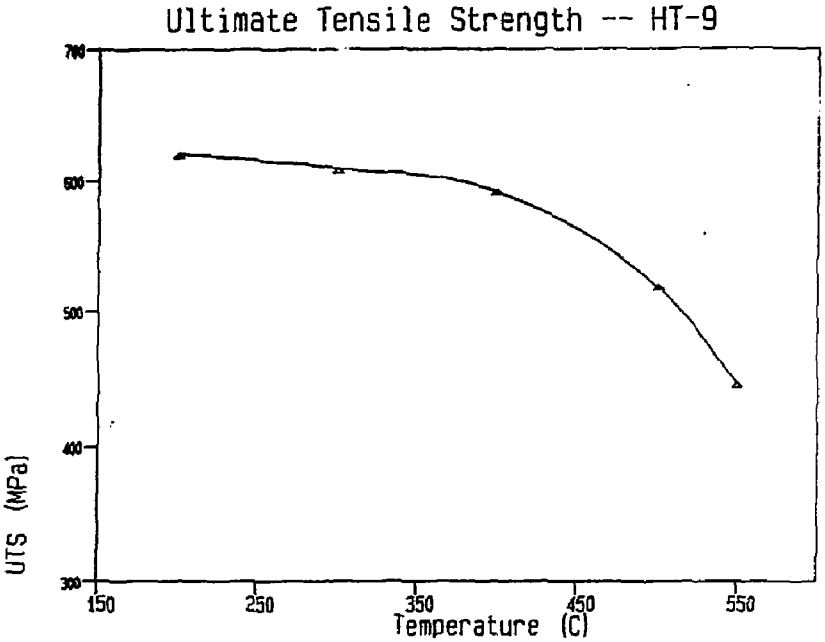
Ultimate Tensile Strength -- HT-9
700
600
500
400
300
UTS (MPa)
150
250
350
450
550
Temperature (C)

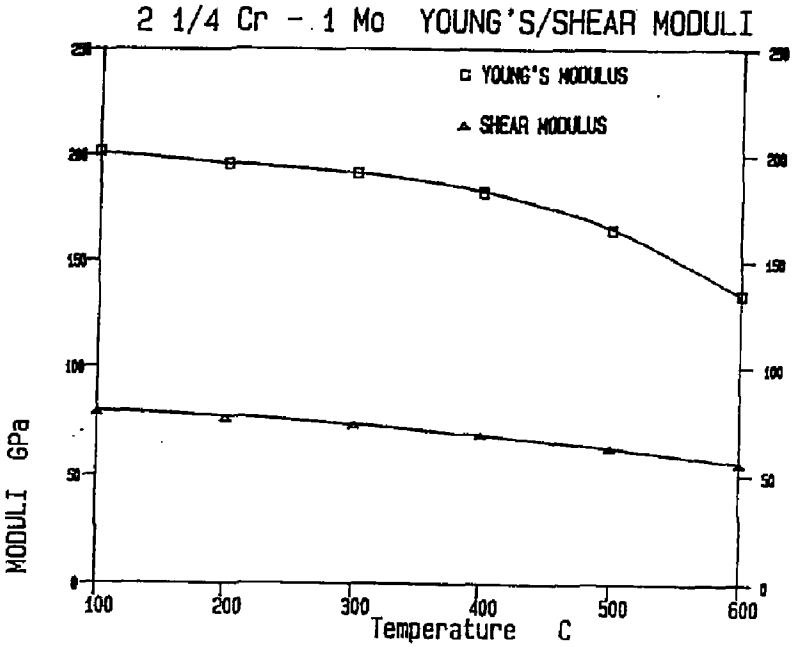
2 1/4 Cr - 1 Mo YOUNG'S/SHEAR MODULI
YOUNG'S MODULUS
SHEAR MODULUS
MODULI GPa
Temperature C
100
200
300
400
500
600

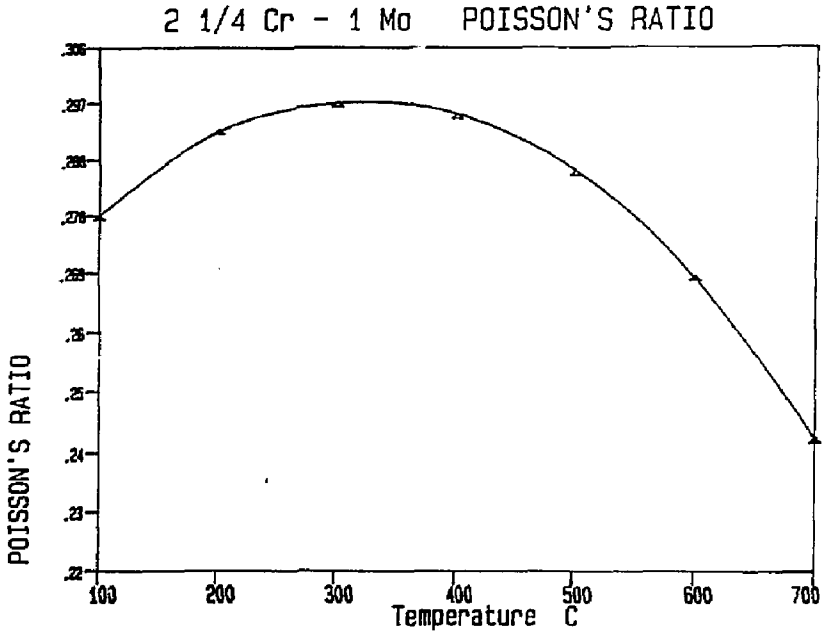
2 1/4 Cr - 1 Mo POISSON'S RATIO
POISSON'S RATIO
Temperature C
100
200
300
400
500
600
700

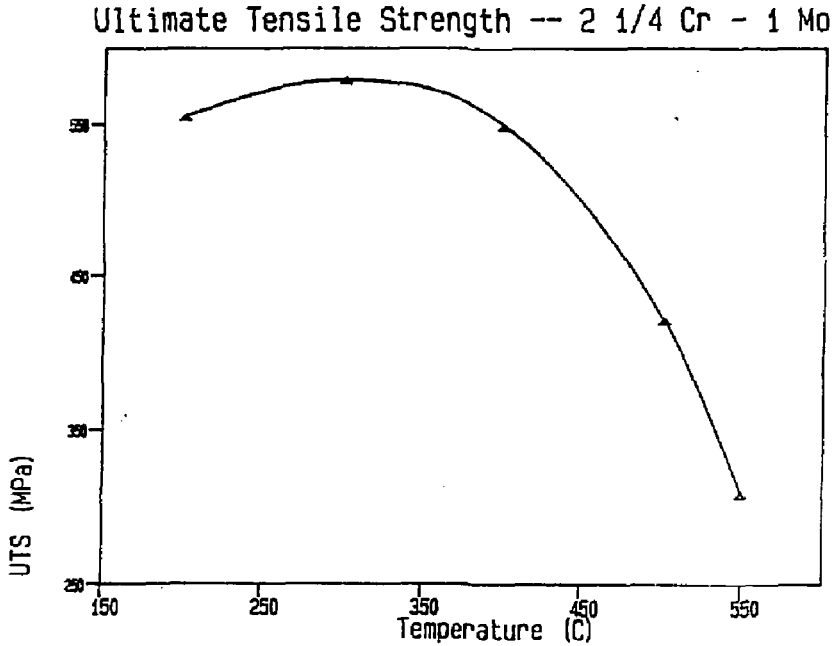
Ultimate Tensile Strength -- 2 1/4 Cr - 1 Mo
UTS (MPa)
250
350
450
550
150
250
350
450
550
Temperature (C)

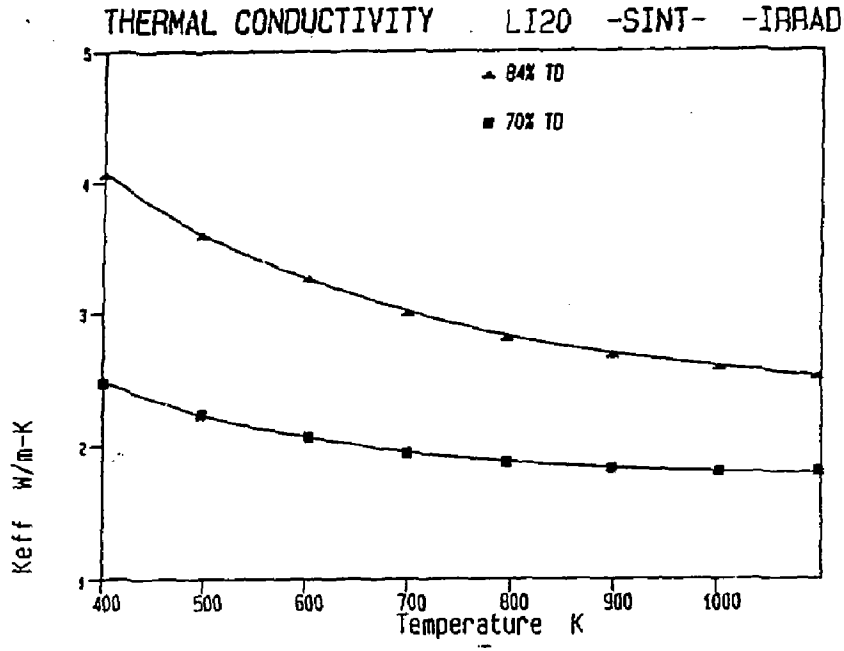
THERMAL CONDUCTIVITY LI2O -SINT- -IRRAD-
84% TD
70% TD
Keff W/m-K
Temperature K
400
500
600
700
800
900
1000

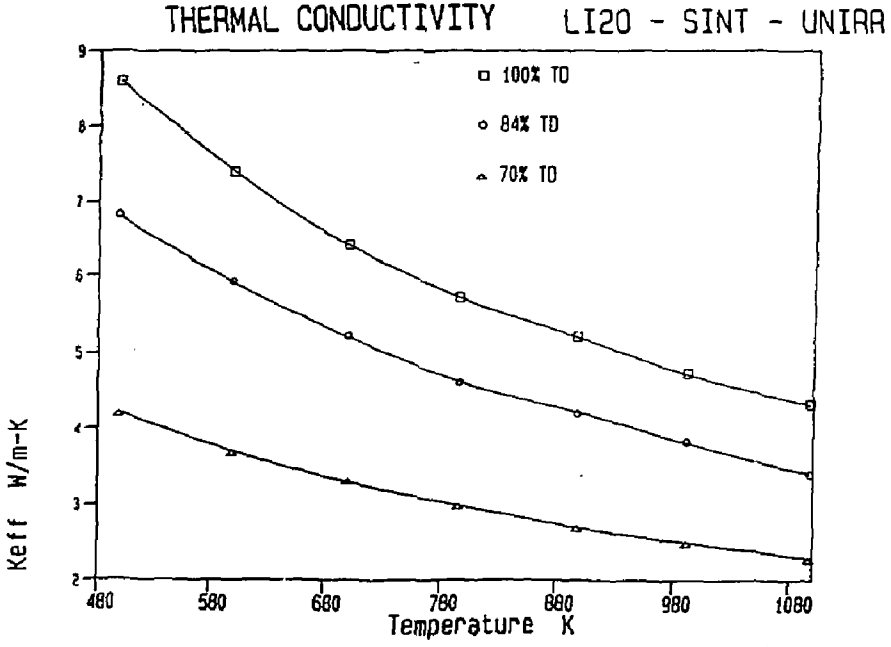
THERMAL CONDUCTIVITY LI2O - SINT - UNIRR
100% TD
84% TD
70% TD
Keff W/m-K
Temperature K
480
580
680
780
880
980
1080

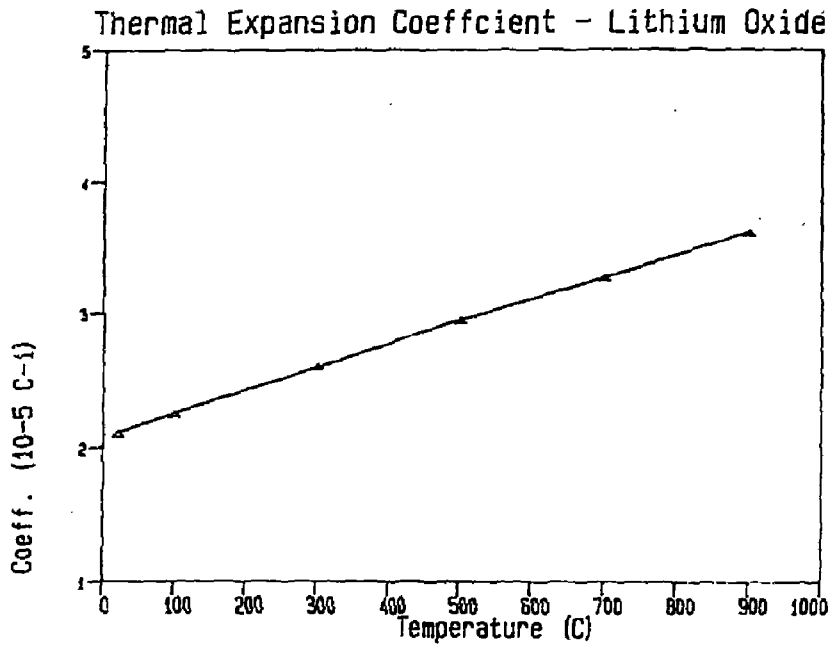
Thermal Expansion Coeffcient - Lithium Oxide
Coeff. (10-5 C-1)
5
4
3
2
1
0
100
200
300
400
500
600
700
800
900
1000
Temperature (C)

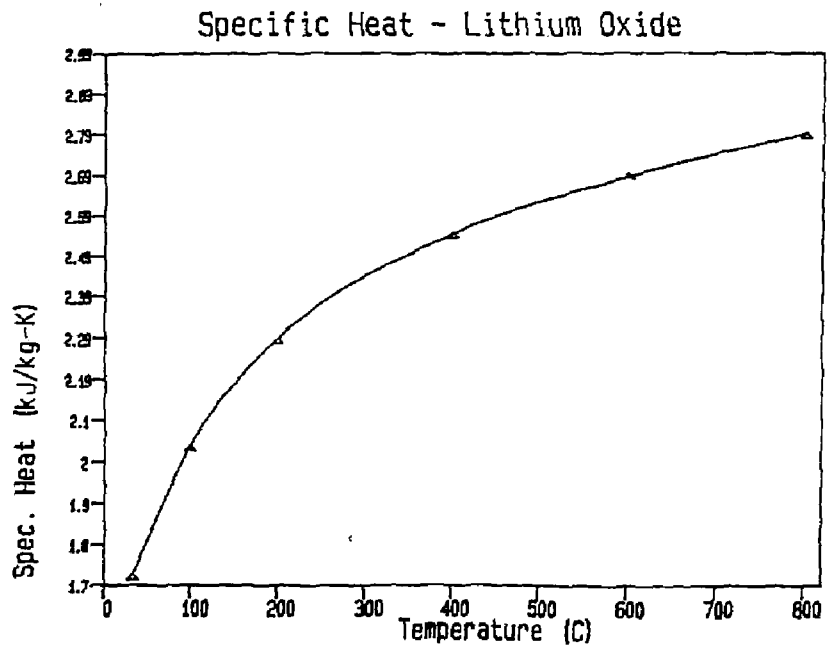
Specific Heat - Lithium Oxide
Spec. Heat (kJ/kg-K)
2.1
2
1.9
1.7
0
100
200
300
400
500
600
700
800
Temperature (C)

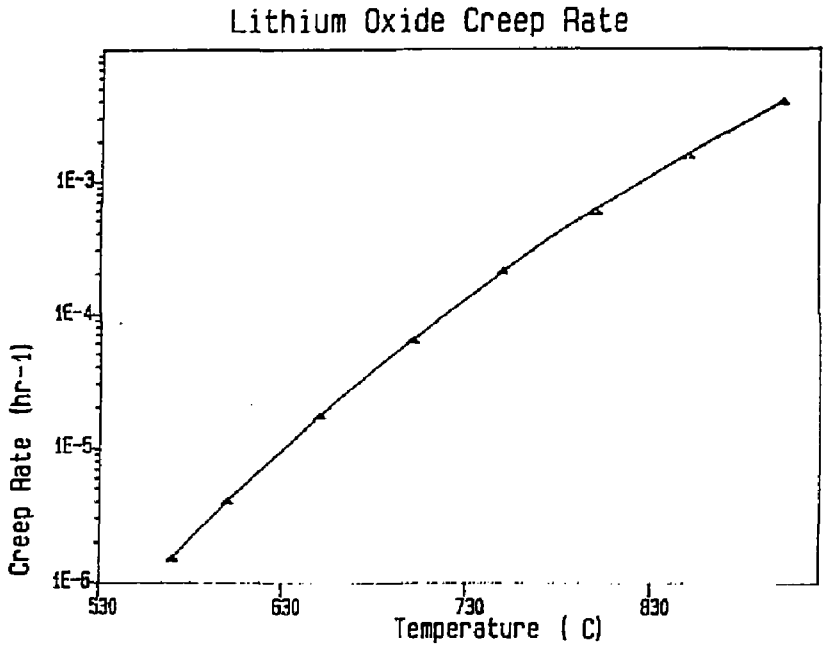
Lithium Oxide Creep Rate
Creep Rate (hr-1)
1E-3
1E-4
1E-5
1E-6
530
630
730
830
Temperature (C)

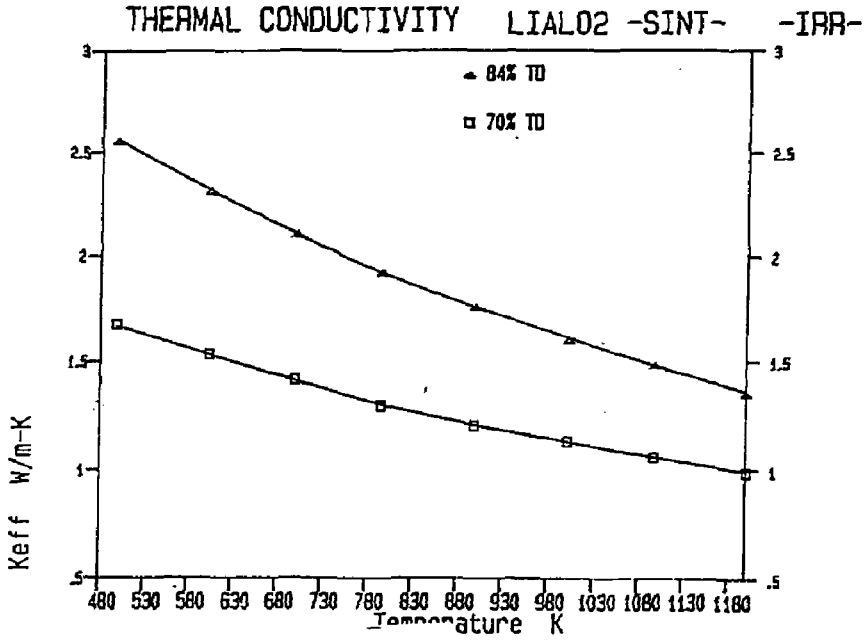
THERMAL CONDUCTIVITY LIALO2 -SINT- -IRR-
84% TD
70% TD
Keff W/m-K
480 530 580 630 680 730 780 830 880 930 980 1030 1080 1130 1180
Temperature K

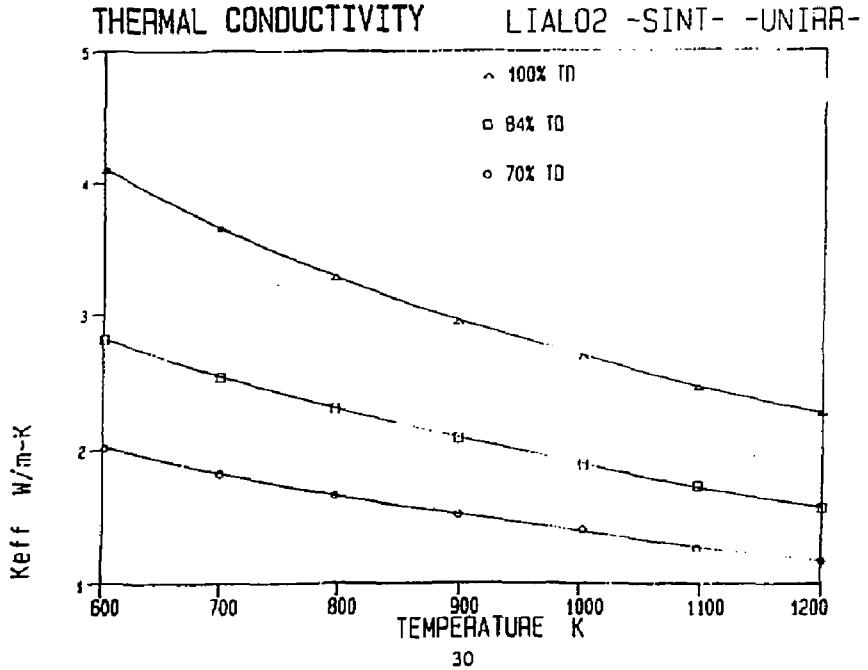
THERMAL CONDUCTIVITY LIALO2 -SINT- -UNIRR-
100% TD
84% TD
70% TD
Keff W/m-K
600 700 800 900 1000 1100 1200
TEMPERATURE K

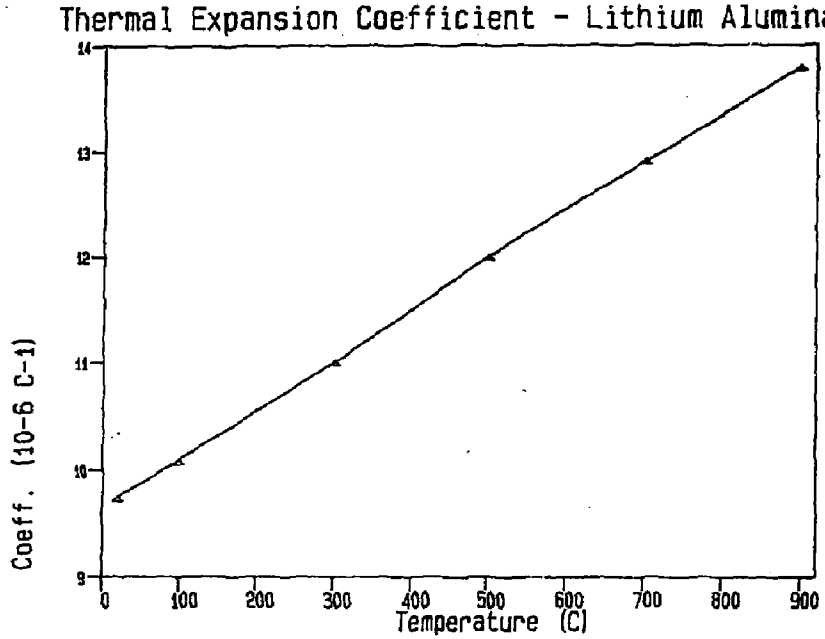
Thermal Expansion Coefficient - Lithium Aluminate
Coeff. (10-6 C-1)
14
13
12
11
10
9
0
100
200
300
400
500
600
700
800
900
Temperature (C)

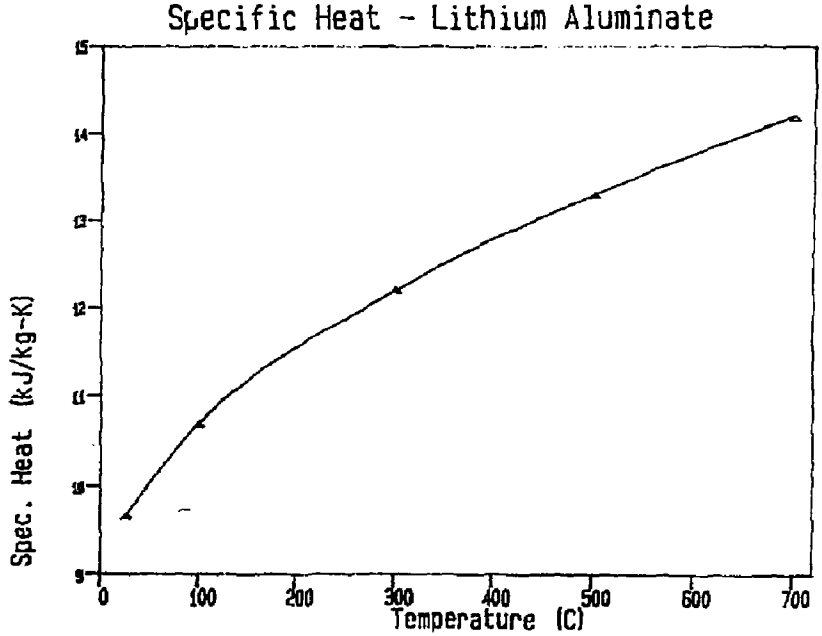
Specific Heat - Lithium Aluminate
Spec. Heat (kJ/kg-K)
15
14
13
12
11
10
9
0
100
200
300
400
500
600
700
Temperature (C)

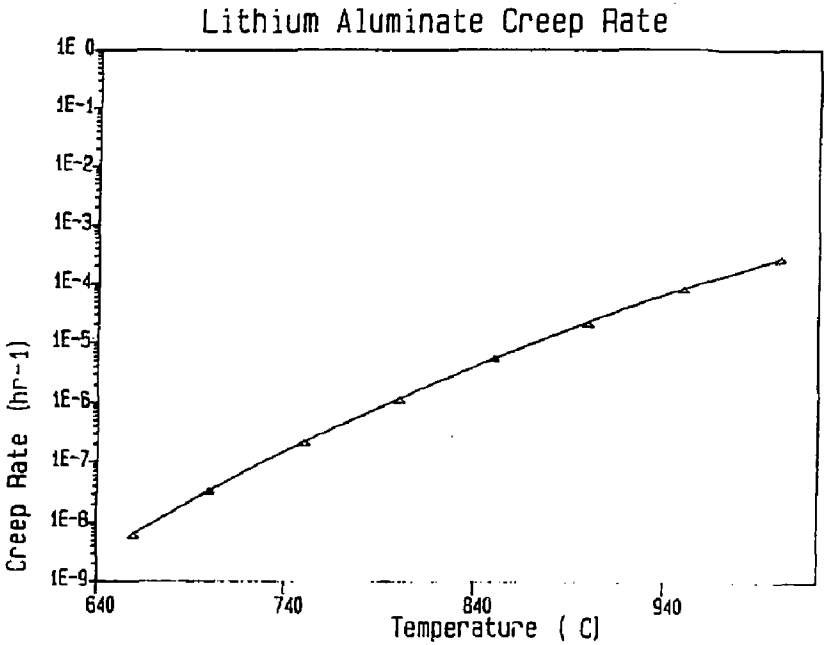
Lithium Aluminate Creep Rate
1E 0
1E-1
1E-2
1E-3
1E-4
1E-5
1E-6
1E-7
1E-8
1E-9
Creep Rate (hr-1)
640
740
840
940
Temperature (C)

4. PHENOMENOLOGICAL SWELLING EQUATIONS FOR SOLID BREEDER AND NEUTRON MULTIPLIER MATERIALS

4.1 Theory

The behavior of Solid Breeder Materials under irradiation has been the subject of various experiments. Hollenberg (2) conducted experiments on Li_2O, $LiAlO_2$ and Li_4SiO_4 ceramics in the FUBR-1A experiment in EBR-II. He reported results on helium retention and swelling of these materials after ≈1% Li burnup (≈$3x10^{20}$ captures/cm^3) as a function of irradiation temperature. Figure 1 shows the percent helium retentions in Li_2O and $LiAlO_2$.

In Li_2O. helium retention is a strong function of temperature, in $LiAlO_2$, however, almost no temperature dependence was detected. Furthermore compared to Li_2O, γ-$LiAlO_2$ has very low helium retention capabilities. The cause of swelling is believed to be helium bubbles forming during irradiation. Thus the different retention rates of helium in LiO_2 and γ-$LiAlO_2$ manifest themselves into different swelling rates. Fig. 2 lends some qualitative support for the relationship between helium retentions and swelling. However, the low and athermal helium retention behavior in γ-$LiAlO_2$ are not known at present. Microstructure examination is needed to ascertain the helium bubble morphology in order to explain experimental findings. Since it is believed that swelling has its microstructural origin in helium behavior, we will develop a simple swelling equation based on the following gas behavior assumptions:

* All retained gas is trapped in bubbles
* All bubbles are of the same size
* Van der Waal's Equation of State (EOS) is used
* Bubbles are in mechanical equilibrium with the solid

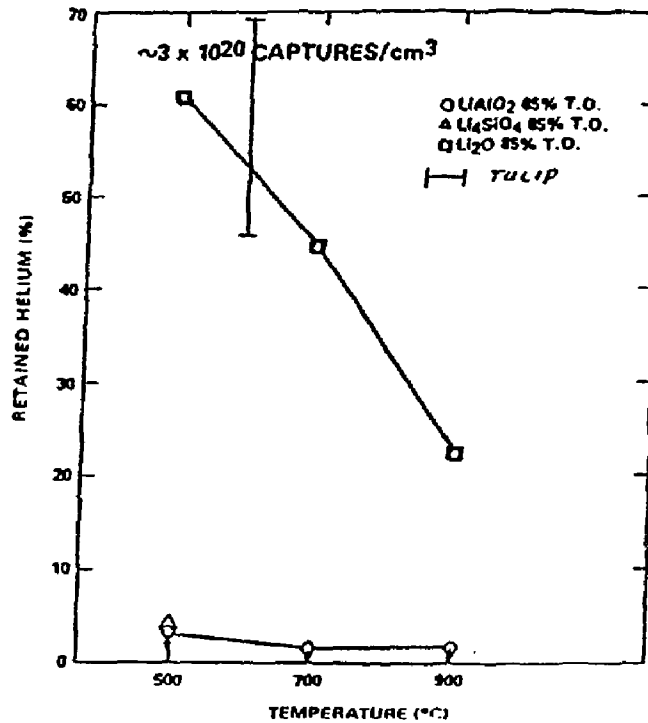

Fig. 1: Helium Retention in the FUBR-1A Experiment (After Hollenberg [2]).

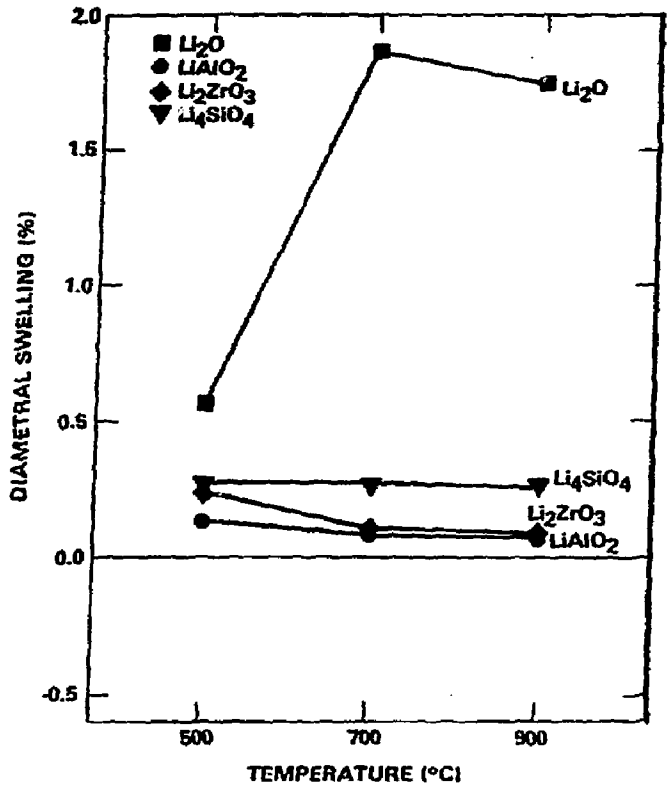

Fig. 2: Diametrical Swelling of Li_2O, Li_4SiO_4, Li_2ZrO_3 and $LiAlO_2$ After Achieving a Burnup of $3x10^{20}$ captures/cm^3 (After Hollenberg [2]).

* Re-solution is neglected

The Van der Waal's EOS is most commonly used to describe the thermodynamic state of fission gases in bubbles. It can be written as

$$p\left(\frac{1}{\rho_g} - B\right) = kT \qquad (1)$$

where p is the pressure of a gas of molecular density ρ_g at temperature T. The van der Waal's parameter B can be regarded as an expression for the volume occupied by the gas atom. Assuming no hydrostatic stress, the mechanical force balance on a bubble dictates that:

$$p = \frac{2\gamma}{R} \qquad (2)$$

where γ is the surface tension of a bubble with radius R. Eliminating pressure between equation (1) and (2), we get for the gas density of a bubble:

$$\frac{1}{\rho_g} = B + \left(\frac{kT}{2\gamma}\right)R \qquad (3)$$

The number of gas atoms (m) contained in a bubble of radius R is

$$m = \left(\frac{4}{3}\pi R^3\right)\rho_g \qquad (4)$$

or using Eq. 3

$$m = \frac{4\pi R^3/3}{B + \left(\frac{kT}{2\gamma}\right)R} \qquad (5)$$

If the functional swelling is small, we can express swelling ($\Delta V/V$) due to gas bubbles by

$$\frac{\Delta V}{V} = \left(\frac{4\pi R^3}{3}\right)N \qquad (6)$$

where N is the bubble number density. We are assuming that all retained helium atoms are trapped inside bubbles of equal size. Thus we can relate

the numbe of gas atoms per bubbles to N by

$$f_R \dot{G}_{He} t = mN \qquad (7)$$

where f_R is the fraction of helium atoms retained and $\dot{G}_{He}$ is the helium production rate and t is the time into irradiation. Combining equation (5), (6) and (7) we can express the swelling due to retained helium atoms produced during irradiation time t:

$$\frac{\Delta V}{V} = \left[\frac{3}{4\Pi}\right]^{1/2} \left[\frac{kT}{2\gamma} \frac{f_R \dot{G}_{He} t}{N^{1/3}}\right]^{3/2} \qquad (8)$$

4.2 Swelling of Solid Breeder Material

Thus we have an expression for swelling as a function of temperature, helium production rate and irradiation time. Note that swelling scales as $t^{1.5}$ which is commonly found experimentally.

To use eq. (8), knowledge about the helium number density is required. The experiment [2] provides us with three swelling data points. Using an approximate value of ≈1000 ergs/cm^2 for bubble surface tension, we find from eq. (8) and the experimental value for swelling and helium retention at 700°C a bubble number density of $N \approx 1.5 \times 10^{-14}$ cm^{-3}. Using Eq. 6, we can now estimate the average bubble radius at specified temperatures. Table 2 shows the estimates for N and R using the experimental data points [2].

TABLE 2

Estimates for bubble number densities
and radii using above model and
experimental swelling data [2] for $LiAlO_2$

T (°C)	*ΔV/V (%)	R (Å)	N x 10^{-14} (cm^{-3})
500	0.12	192	0.382
700	0.09	112	1.533
900	0.07	69	5.017

* Experimental data

Assuming a temperature insensitive bubble number density for 500 ≤ T ≤ 900 °C we find a slight increase in swelling as a function of temperature, while experimental evidence points to a slight decrease. In Table 3 we compare experimental to analytical results.

TABLE 3

Experimental [2] and Analytical [Eq. 8]
Swelling Results for $LiAlO_2$ for 500 ≤ T ≤ 900 °C

T(°C)	ΔV/V (%) Exp.	Anal.
500	0.12	0.015
700	0.09	0.092
900	0.07	0.122

We can now estimate swelling rates of $LiAlO_2$ for our blanket conditions. As a demonstration of our model we can use a helium generation rate of about $5x10^{13}$ $He/cm^3/sec$, typical for 5 MW/m^2 neutron wall loadings. Furthermore we assume a bubble number density of about $1.5x10^{14}$ cm^{-3} and an athermal helium retention fraction of 3%. Fig. 3 shows the results of our phenomenological equation. Under these conditions the swelling is estimated

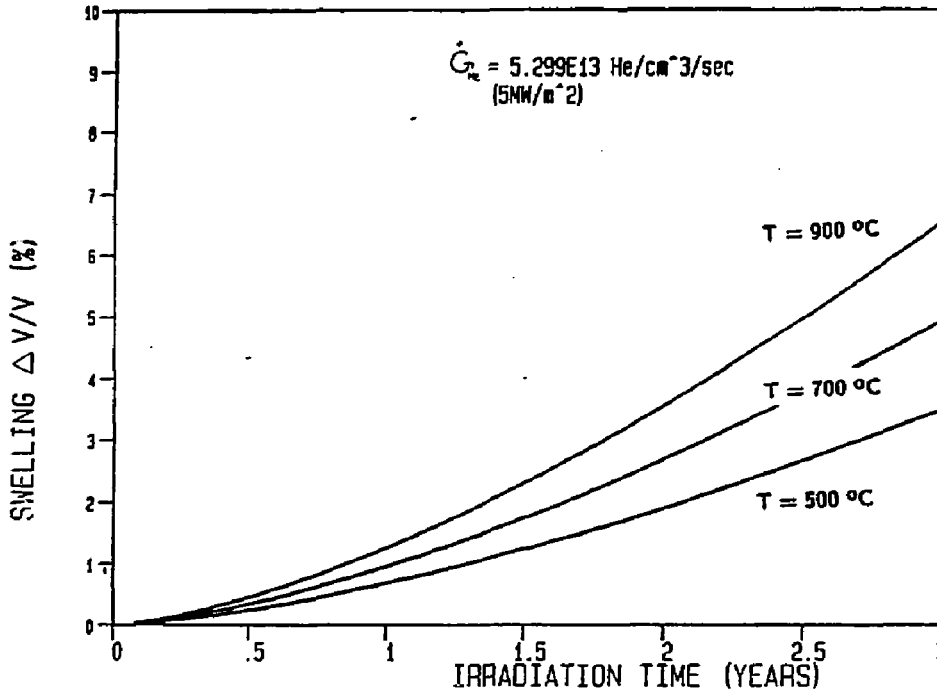

Fig. 3: Volumetric Swelling of $LiAlO_2$ Exposed to ≈ 5 MW/m^2 of Neutron Wall Loading as a Function of Irradiation Time.

to ≈ 6.7% at 900 °C and 3.3% at 500 °C after 3 years of irradiation.

Using the approach outlined above, we have also used Hollenberg's experimental swelling data for Li_2O [2]. Table 4 shows the experimental findings for swelling and helium retention at various temperatures.

TABLE 4

Experimental swelling and helium retention data [2] for Li_2O

T (°C)	ΔV/V (%)	f_r (%)
500	0.6	60
700	1.8	43
900	1.6	20

The model combined with these experimental data points allows us to estimate the bubble number density (N) and bubble radii (R). Table 5 shows these estimates.

TABLE 5

Estimate for bubble number densities and radii using the above model and experimental data [2] for Li_2O

T (°C)	* ΔV/V (%)	R(Å)	$Nx10^{15}$ (cm^{-3})
500	0.6	61.5	6.19
700	1.8	195	0.58
900	1.6	323	0.12

* Experimental values

We see an increase in bubble radius as a function of temperature for Li_2O, while for $LiAlO_2$ (Table 2) we note a decrease in bubble size. This is

consistent with the swelling results measured by Hollenberg [2]. In $LiAlO_2$ thermal emission of helium atoms from bubbles is probably the major cause for bubble shrinkage thus leading to a decrease in swelling with increasing temperatures. Our model does not reflect this behavior because of the simplifying assumptions we had to make due to lack of knowledge of helium behavior in ceramics. We are assuming constant size and constant bubble densities in describing the swelling behavior. These assumptions are more justified for Li_2O ceramics since swelling more than doubles over the 500 to 900 °C temperature range. Thus our model's predictions are in better agreement for Li_2O than for $LiAlO_2$. Table 6 compares our model result to experimental data.

TABLE 6

Experimental [2] and analytical [eq. 8] swelling results for Li_2O for $500 < T < 900°C$

	ΔV/V (%)	
T (°C)	Exp.	Anal.
500	0.6	0.58
700	1.8	1.65
900	1.6	1.55

Experimental data for Li_2O show a highly temperature sensitive swelling rate and helium retention fraction. Because of this we no longer can assume constant bubble number densities and retention fractions without introducing large errors in the model. Because of this, we have used the values of Table 4 to evaluate swelling rates for Li_2O at the various temperatures. The results of applying our swelling equation (eq. 8) to our reactor conditions are demonstrated in Fig. 4. We find our model to follow experimental trends predicting a slightly higher swelling rate for 700°C than for 500 or 900 °C.

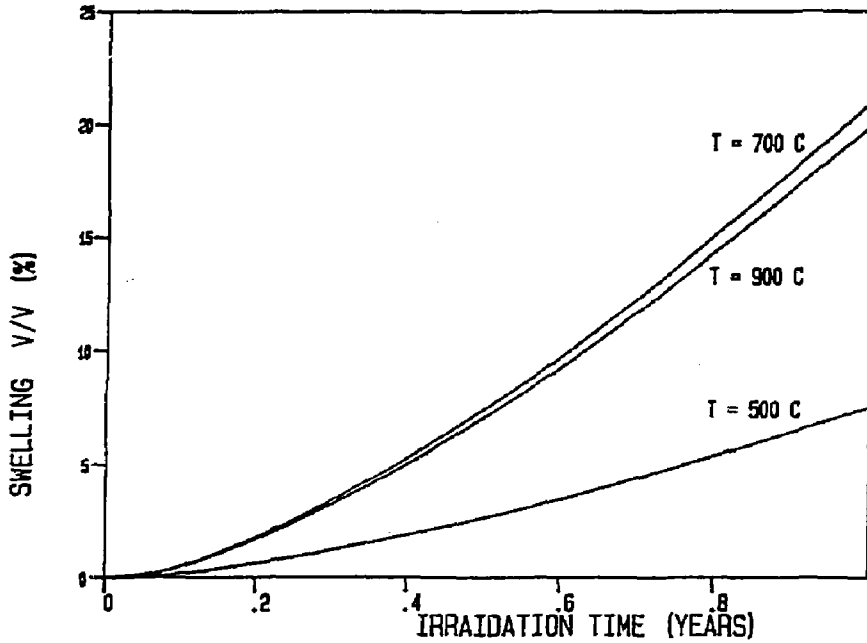

Fig. 4: Volumetric Swelling of Li_2O Exposed to ≈ 5 MW/m^2 of Neutron Wall Loading as a Function of Irradiation Time.

For our model to be used at intermediate temperatures between 500 and 700°C, one could use a simple linear extrapolation of the bubble number densities and fraction of helium retained from Tables 4 and 5.

It should be noted, however, that our approach is purely a phenomenological one, which does not necessarily take into account the actual physical behavior of helium atoms in ceramics under irradiation. Our model does not include important parameters such as porosity, grain size, dislocation network or irradiation produced damage. A model describing these phenomena would require a major effort combining experiment with basic analytical research over a period of many years.

4.3 Beryllium Swelling

The swelling equation (eq. 8) can also be applied to beryllium. Beryllium has a large (n,2n) reaction associated with helium production. Furthermore, the 14 MeV neutrons create high PKA energies. Because of these characteristics, swelling is of major concern in beryllium. Effects of helium production and irradiation-induced dimensional changes in Be have been the subject of experimental investigations using fission spectrums by Beeston and coworkers [10, 11]. They irradiated Be-specimens in ETR and ATR up to 3.5×10^{22} n/cm^2 (E > 1 MeV). Beeston's et. al. [10,11] measurements represent low neutron energy, low fluence irradiation conditions. Because the effects of fast neutron, high fluence irradiation are not known at the present time, we have to base our model on Beeston's data. Thus our simple model, although applicable to fission conditions, has to be used cautiously when applied to fusion conditions. As was the case before, we need to know the bubble number densities, the fraction of helium atoms retained and the surface energy of beryllium.

Beeston gives an empirical equation for the number density of helium

bubbles for an annealing temperature between 400° and 600°C.

$$N = 1.4 \times 10^{14} \exp(0.45/kT) \quad cm^{-3} \qquad [9]$$

No measurements for the fraction of helium atoms retained were reported. Thus we will take the conservative approach of trapping all produced helium atoms inside the bubbles. Surface energy measurements quote values ranging from 1 to 2 J/m^2 [12, 13, 14]. Wolfer et. al. [15] have also investigated beryllium swelling behavior. They [13] use a similar simple swelling model and report best agreement between model and data for a surface energy value of 2 J/m^2. Thus we will use the 2 J/m^2 value for the surface energy of beryllium in our model. Table 7 compares Beeston's data [10,11] to our model.

TABLE 7

Experimental [10,11] and analytical swelling results for Be irradiated to 50,000 appm at 400° < T < 600°C

	ΔV/V (%)	
T (°C)	Exper.	Analyt.
400	5	4.54
450	9	6.61
500	12	9.24
550	17	12.5
600	20	16.4

We have applied the simple swelling model to the present blanket design. Fig. 5 shows the average pin temperature as a function of distance from the first wall. The maximum Be-pin temperature is ≈ 440°C while the $LiAlO_2$ hottest pin reaches ≈ 1000°C. The six Be-pins are all of the same

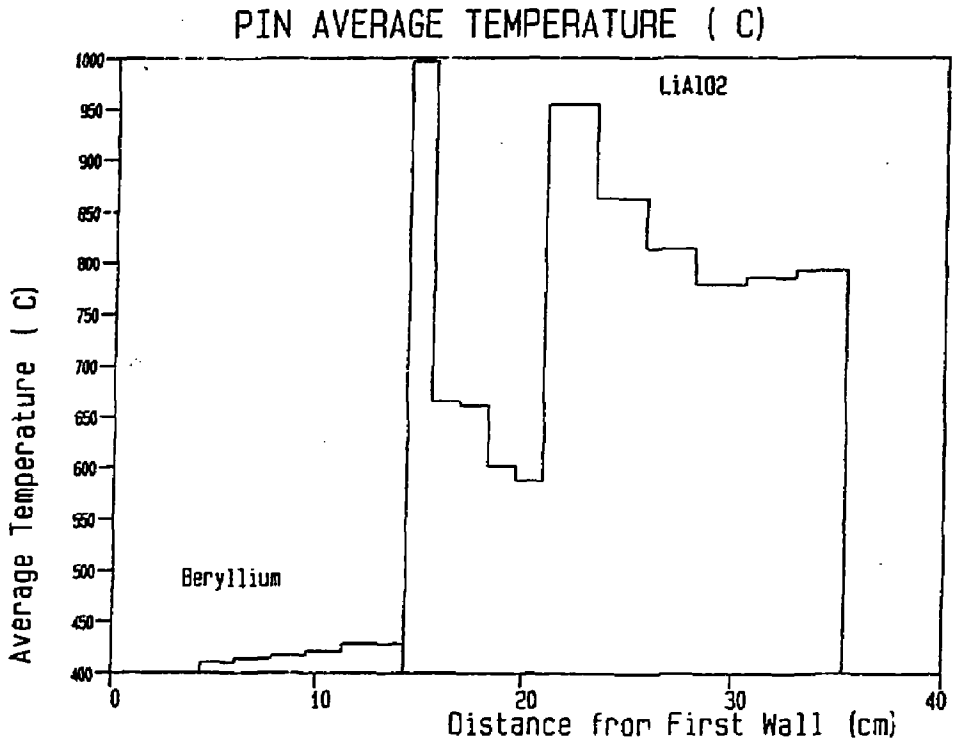

Fig. 5: Blanket Pin Average Steady State Temperature as a Function of Distance from the First Wall for a Neutron Wall Loading of ≈ 5 MW/m^2.

size. The five front $LiAlO_2$ pins are roughly half the size of the following six rows of breeder pins. Fig. 6 shows the helium atom production rate in the $LiAlO_2$ pins as a function of distance from the first wall. The helium atom production rate in the beryllium rods is depicted in Fig. 7. Note that the helium production rate is roughly an order of magnitude larger in Be than it is in the breeder pins.

In Fig. 8 we have shown the volumetric swelling of the $LiAlO_2$ breeder pin at the end of three years. We have assumed a constant helium atom production rate. Thus not allowing for burnup of lithium atoms. Nevertheless, the maximum swelling occurs in the front row of breeder pins with a top value of $\simeq$ 1.3 % after 3 years. This level of swelling would be tolerable for blanket lifetimes of 3 - 4 years.

The high helium-generation rate in Be-rods turns out to be the life limiting phenomena for our blanket design. In Fig. 9 we have depicted the beryllium volumetric swelling at various irradiation times. After 1 year of irradiation the maximum swelling occurring in the first row of Be-rods reaches 7.7%. This value increases to unacceptable limits of 20 and 30% after 2 and 3 years respectively. Although these levels of swelling seem to limit the blanket lifetime to about one year, one should note that no allowance was made for Be-burnup during the irradiation time. Furthermore, at high levels of swelling, microstructural evolutions will play an important role. High swelling rates coupled with thermal cycling lead to the formation and propagation of cracks. If bubbles form predominately on grain boundaries, interlinkage of bubbles can lead to gas releases high enough to reach swelling peaks. Another important microstructural evolution is the role of dislocation network formation during irradiation. Dislocations can sweep bubbles from the matrix to grain boundaries, or act as gas tunnelling

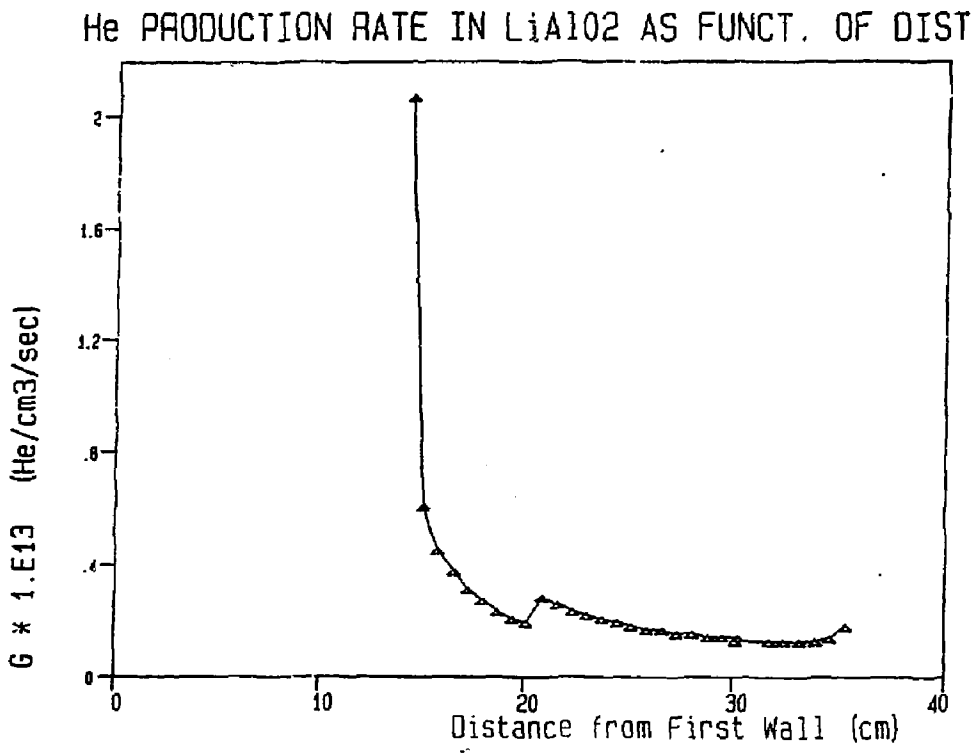

Fig. 6: Helium Production in $LiAlO_2$ Breeder Pins as a Function of Distance from the First Wall.

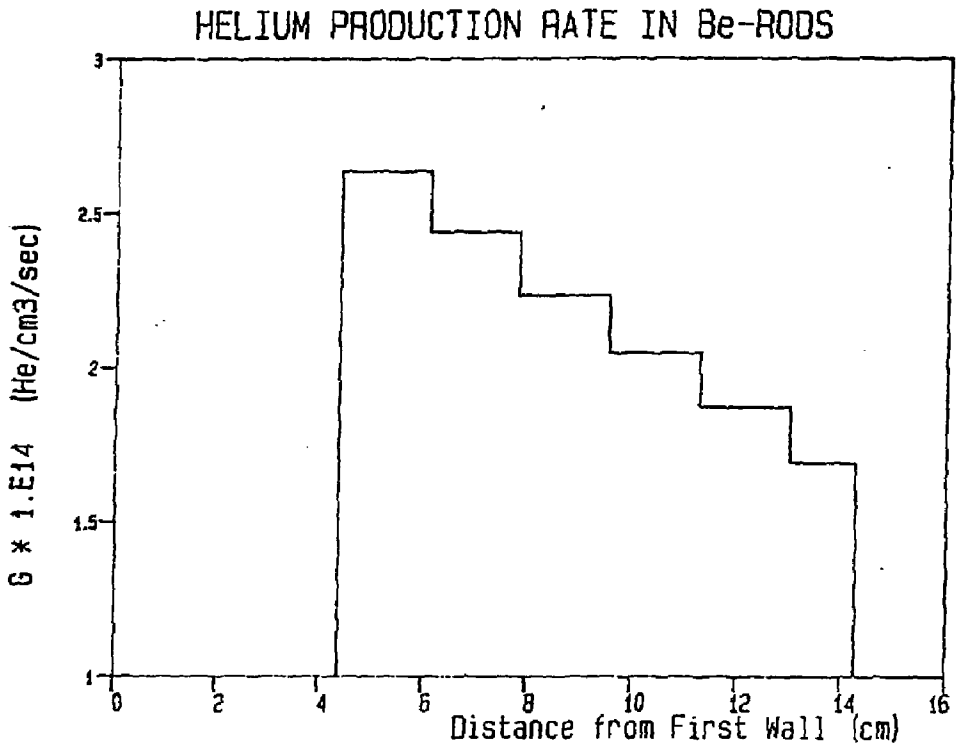

Fig. 7: Average Helium Production in Be-Rods as a Function of Distance from the First Wall.

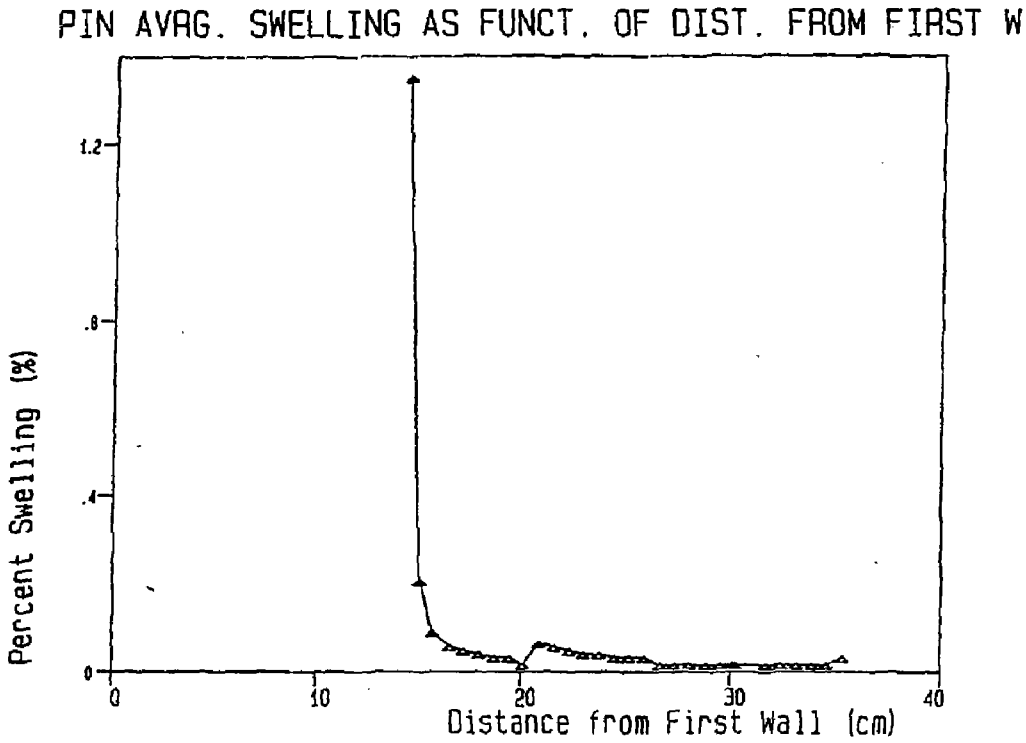

Fig. 8: Average Volumetric Swelling of $LiAlO_2$ - Breeder Rods Exposed to 5 MW/m^2 Neutron Wall Loading after 3 Years of Irradiation.

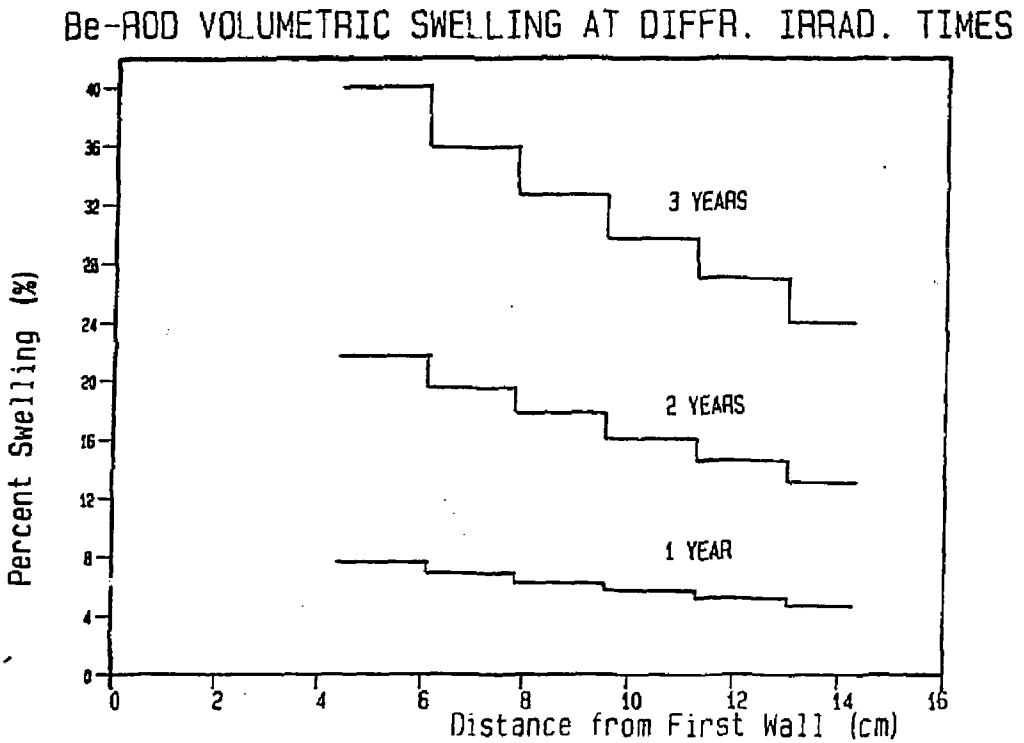

Fig. 9: Volumetric Swelling of Be-Rods Exposed to 5 MW/m^2 Neutron Wall Loading after 1,2 and 3 Years of Irradiation.

channels. Both phenomena lead to an increase of gas release from the matrix. Furthermore, dislocation climb is considered a major creep mechanism that can accommodate volumetric swelling. Due to lack of consideration of microstuctural phenomena, the high swelling rates for Be-rods cannot be considered accurate. They only point to a potential problem which has to be investigated in great detail experimentally and analytically.

5. Sintering Phenomena in Breeder Ceramics

5.1 Introduction

Two configurations for solid breeders have been considered: pressed and sintered pellets and sphere-pac. Cold pressing and sintering techniques were developed for Li_2O, Li_4SiO_4, and γ-$LiAlO_2$ samples irradiated in ORR [16] and EBR-II irradiation experiments [17].

For LWR and fast reactor fuel rods sphere-pac technology has been developed and is considered attractive for solid-breeders.

The sphere-pac solid breeder configuration could potentially allow for higher thermal conductance due to the elimination of pellet clad gaps. This configuration assumes that internal shifting of the sphere-pac will accommodate expansions or contractions of solid breeder material.

A sound understanding of the factors that govern the temperature distribution within the solid-breeder material is essential to successful prediction of breeder performance over long periods of time and in an intense radiation field.

The temperature distribution, which depends strongly on porosity, influences solid-breeder performance in two important ways:

1. High temperatures: Solid-state reactions that would be immeasurably slow at lower temperatures proceed at rates sufficient to produce significant changes in material properties during the life-time of the breeder in the reactor.

   Phenomena primarily affected by high operating temperatures include:

   a. Grain growth
   b. Densification (sintering)

c. Fission-product diffusion

2. Steep temperature gradients: High temperatures can close pores which migrate up a temperature gradient; important constituents of solid-breeder material, such as oxygen, Li, and fission products, are redistributed from their initial concentration profiles (which are usually uniform); thermal stresses resulting from the temperature gradients cause breeder material either to deform plastically in regions of high temperature or to crack in low-temperature zones.

Because porosity determines both temperature and temperature gradients in solid breeders, the next section will outline some effects of porosity.

The following section looks at the possibility of sintering of sphere-pac solid breeder material.

5.2 The Effect of Porosity

Oxide fuels are generally fabricated by sintering pellets of pressed powdered UO_2 or mixed UO_2-PuO_2 at high temperatures (typically 1700 °C) for a predetermined length of time. By control of the sintering conditions, materials of any desired density between 80 and 90% of theoretical density can be produced.

In the sphere-pac route, high density ceramic spheres of controlled sizes are produced and then subsequently loaded with the assistance of low-energy vibration.

The high density ceramic spheres are produced in three steps:

1. Preparation of a special solution
2. Gelation of droplets to give semi-rigid spheres
3. Drying and sintering these spheres to a high density.

Inasmuch as porosity in a ceramic body invariably reduces its thermal conductivity, it would appear desirable to eliminate all internal pores or voids in the fuel fabrication process.

However, a certain amount of fabricated porosity is useful in accommodating the fission products that accumulate during irradiation; porosity is a means of minimizing fuel swelling. The density of both thermal and fast reactor fuels are well below theoretical value. The porosity of the fast reactor [(U, Pu) $O_{1.96}$, $\rho \approx 90\%$ TD] is purposely made greater than that of the thermal reactor fuel [$UO_{2+x} \approx 92\%$ TD], because of the larger burnups required in the former. (Larger burnups are required to enhance breeding-ratios

Since controlled solid breeder material porosity is a design variable, it is important to be able to predict the effect of porosity on solid-breeder properties, in particular on thermal conductivity and consequently fission gas (^3T) diffusivity.

Theoretical analysis of the effect of porosity on thermal conductivity has been hampered by the number of variables that must be considered. One variable that appears in most theoretical models is the volume porosity (P), defined by:

$$P = \frac{\text{volume of pores}}{\text{volume of pores + volume of solid}}$$

In addition, the geometry and physical properties of the individual pores may also be important. Pore geometry is defined by its size, shape and orientation with respect to the direction of heat flow. Physical properties that may be significant are the emmisivity of the solid and the thermal conductivity of the gas trapped within the pore (if any).

In 1954, Loeb [18] treated the thermal conductivity in a manner that permitted many of the secondary variables mentioned in the preceding

paragraph to be properly accounted for. In 1966, Biancheria [19] was able to theoretically account for the effects of pore shape.

The well-known Loeb equation describing conductivity of a porous material is:

$$k = k_s(1-P) \tag{9}$$

where k - thermal conductivity of a porous material

k_s - thermal conductivity of a solid material

P - porosity given by

$$P = 1 - \left(\frac{\rho}{\rho_s}\right) \tag{10}$$

where $\frac{\rho}{\rho_s}$ is percentage of theoretical density.

Loeb's equation has been found to underestimate the porosity effect on the thermal conductivity of UO_2. This deficiency has been remedied by inserting an adjustable parameter to yield:

$$k = k_s(1-\alpha P) \tag{11}$$

Equation (11) is called the modified Loeb equation. Values of the parameter α from 2 to 3 have been determined by fitting this equation to UO_2 thermal-conductivity measurements.

Biancheria's [19] analysis of the porosity effect yield the following formula:

$$\frac{k}{k_s} = \frac{1-P}{1+(\alpha-1)P} \tag{12}$$

However, contrary to the purely empirical nature of the parameter α in equation (11), α in equation (12) can be evaluated for equal-sized pores of a particular geometry randomly distributed in the solid. For spheres

α = 1.5; for axisymmetric shapes such as ellipsoids of revolution, the sphere factor α is greater than 1.5.

In theory, the thermal conductivity of porous ceramics can be determined by using equations 9, 11 or 12. However, extensive measurements of UO_2 thermal conductivity have shown that the theoretical formulas do not agree well enough with experiments to serve as design equations.

This trend will probably hold true for solid-breeder material and purely empirical formulas should be used when reliable numerical values are needed.

Yung Y. Liu, M.C. Billone and R. Clemmer [20] have performed thermal-conductivity measurements on irradiated and unirradiated Li_2O-sintered pellet and sphere-pac γ-$LiAlO_2$, which could be utilized to compare to theoretical values and to produce empirical equations for k_{eff} of Li_2O and γ-$LiAlO_2$.

5.3 Sintering

Lithium oxide pellets in the form of cylinders with 1 in. in diameter by 1 in. in height have been prepared for the TFTR lithium blanket module (LBM) program [21].

To facilitate the release of bred tritium, the density of these pellets is purposely kept well below theoretical densities (TD). Takahashi and Kikuchi [22] have demonstrated that as the density of Li_2O pellets is increased above 86%, the fraction of closed porosity remains essentially constant at 3% to 4% of the pellet volume.

Sphere-pac requires three sizes of spheres to achieve about 88% smear density. If a lower density is acceptable, two sizes will yield

about 85% smear density [23].

The contact area between adjacent microsphere plays an important role in the thermal conductivity. Although there is only a ≈3% difference in density between ternary and binary mixtures of UO_2, experiments [24] show that the effective conductivity of the ternary mixture of UO_2 (1.75 W/m-k) is much higher than that of a binary mixture (0.9 W/m-k).

Fuel-gap conductance has also been measured for sphere-pac fuel and pellets of identical fuel composition [25]). These measurements show a gap conductance of 7.3 kW/m^2 °C for pellet fuel and 19.3 kW/m^2 °C for sphere-pac fuel. This reduction of contact resistance between the breeder and its clad can significantly change temperature distributions of the breeder material.

From the point of view of thermal conductivity and lithium loading in the blanket, the density of the solid breeder material should be maximized, whereas from the point of view of tritium recoverability porosity, in particular open porosity, should be maximized.

One of the challenges encountered in solid-breeder material design lies in determining this optimum density for the breeder material. Once determined, what will the upper temperature limit be to insure no further densification?

To shed light on some of these issues let us examine some sintering mechanisms which could occur in sphere-pac solid breeder material.

During sintering, an originally porous compact is transformed into a dense ceramic. Most commonly pores become more spherical (i.e., closed) in shape and smaller in size as firing continues. The free energy that gives rise to densification is the decrease in surface area and lowering

of the surface free energy by the elimination of solid-vapor interfaces. This usually takes place with the coincidental formation of new, but lower-energy, solid-solid interfaces. Thus restructuring of the contact area between the microsphere causes a change in shape and shrinkage of the pore.

The different mechanisms for material transfer during sintering processes are:

a. Evaporation and Condensation

b. Viscous flow

c. Surface diffusion

d. Grain-boundary or Lattice diffusion

e. Plastic deformation.

In treating fission fuel material the two mechanisms shown to be important are: Evaporation-Condensation and Diffusion. In the absence of temperature gradients vapor phase material transfer can occur due to vapor pressure differences as a function of particle curvatures.

For micron-range particle size the vapor pressure has to be larger than 10^{-4} - 10^{-5} atm for evaporation-condensation to be significant.

Vapor pressures reach significant values for Li_2O above 1200°C and for $LiAlO_2$ above 1400°C, both well above proposed upper temperature limits.

However, if vapor pressures are low, material transfer may occur more rapidly by diffusion. Diffusion is equivalent to the migration of lattice vacancies in the opposite direction. Material can migrate from the grain boundaries between particle to the neck area between two microspheres resulting in equivalent motion of particle centers toward one another. This results in simultaneous changes in pore size and pore

shape and a corresponding decrease in overall porosity.

Kingerly [26] has derived an expression for the rate of growth of bond formation (x). His finding, $x \alpha t^{1/5}$, are verified experimentally.

$$\frac{x}{r} = \left[\frac{40\gamma D_x \Omega^3}{kT}\right]^{1/5} r^{-3/5} t^{1/5} \tag{13}$$

Using equation (13), Kingerly [26] derived an expression for the shrinkage of a compact:

$$\frac{\Delta V}{V} = 3\left[\frac{20\gamma\Omega^3 D_v}{\sqrt{2}\ kT}\right]^{2/5} r^{-6/5} t^{2/5} \tag{14}$$

From this expression he concluded that shrinkage is not strongly time dependent [$(\Delta V/V) \alpha t^{2.5}$] but size dependent. The sintering rate is roughly proportional to r^{-1} [$(\Delta V/V) \alpha r^{-6/5}$]; as the particle size is decreased, the rate of sintering is raised.

The other variable affecting sintering rates is the vacancy diffusion coefficient which is sensitive to temperature and impurities. Because the vacancy diffusion coefficients have not been well extablished for solid-breeder material use of Kingerly's equations can be misleading in determining sintering behavior of γ-$LiAlO_2$.

Some experimental measurements [27] indicate the onset of sintering in sphere-pac γ-$LiAlO_2$ around 1200°C.

Great uncertainty remains as to the effect of irradiation on the sintering rate.

The kinetics of the sintering process depends on the location of the pores (which are the vacancy sources) relative to the grain boundaries (which are the vacancy sinks). Porosity close to the grain boundaries is

more rapidly eliminated than porosity in the middle of the grain for in the latter case vacancies must diffuse through the bulk.

The rate of shrinkage of a porous solid is governed by the flux of vacancies reaching the grain boundary from the pores.

In Kingery's model, the only means by which vacancies left a pore and entered the adjacent solid was by diffusion.

In solid-breeder material exposed to radiation, however, vacancies can be ejected into the solid by the disruptive action of primary-knock on-atoms (PKA's) passing through or near a pore. This is a type of re-solution process generally associated with fission-gas bubbles. Although a pore can be thought of as consisting of $(4/3)\pi R_p^3/\Omega$ vacancies, the vacancies are not ponderable particles that can acquire kinteic energy by collision with high-speed particles (e.g., a fission fragment or a lattice knock-on). Therefore, pore shrinkage by fission fragments or PKA's must be described by a form of macroscopic re-solution, in which a passing fragment blasts solid from one side of a pore to the other, trapping some acancies in the deposited side in the process. The buried vacancies are considered to be redissolved and to acquire the mobility of single vacancies in the lattice.

Because the pores in ceramic fuels and thus in solid-breeder material are considerably larger than fission-gas bubbles, it is unlikely that a pore can be completely converted to vacancies by a single re-solution event. Hence re-solution is considered to reduce the size of the pores but not to change the total pore concentration. In sphere-pac solid breeder material we have highly dense microspheres with the porosity concentrated in large volumes between the spheres. In this case it is even more unlikely that re-solution will have any effect on the

shape or size of the pores and consequently on the sitering rate.

The other irradiation effect that could be considered is the substantial vacancy production rate due to collision cascades and fission spikes. In densification models neither of the vacancy sinks in the solid (grain boundaries) exhibits a preference for interstitials or vacancies; so an excess of one type of point defect in the solid cannot be built up. Only dislocations are biased sinks, and they are not considered. If they were, swelling rather than shrinkage would probably occur, for this is the prime effect of the presence of dislocation sinks in void swelling in metals.

The above discussion shows that unrealistic assumption concerning the distribution of the pores, their initial size, the neglect of grain growth concurrent with densification, and the effects of radiation on re-solution and pore shape have to be made in order to model sintering of solid-breeder material.

Therefore, we have to rely on experiments to set guide-lines in the development of solid-breeder material.

Acknowledgement

This work was supported by the U.S. Department of Energy, Office of Fusion Energy, Grant #DE-FG03-80ER52061, to UCLA.

References

[1] Materials Handbook for Fusion Energy Systems, DOE/TIC-10122; April 30, 1980; John W. Davis, Coordinator

[2] G.W. Hollenberg, "Fast Neutron Irradiation Results on Li_2O, Li_4SiO_4, Li_2ZrO_3 and $LiAlO_2$", J. Nuclear Materials 122&123 896-900 (1984).

[3] B. Rasneur, "Tritium Breeding Material: γ-$LiAlO_2$", Fusion Technology, Vol. 8, July 1985.

[4] R.J. Amodeo and N.M. Ghoniem, J. Nuclear Materials; Vol. 122, Nos. 1-3; May 1984, p. 91.

[5] R.J. Amodeo and N.M. Ghoniem, "Development of Design Equations for Ferritic Alloys in Fusion Reactors", NED/Fusion 2 (1985) 97-110.

[6] D.S. Gelles and R.J. Puigh, "Alloy Development for Radiation Performance", Semi-Annual Progress Report, DOE/ER/0045/11 Sept. 1983).

[7] N.M. Ghoniem and R.W. Conn, Assessment of Ferritic Steels for Steady State Fusion Reactors", International Atomic Energy Agency, Proc. on Fusion Reactor Design and Technology, IABA-TC-392/62, Vol. II (1983) p. 389.

[8] R.J. Amodeo and N.M. Ghoniem, Development of Design Equations for Ferritic Alloys in Fusion Reactors, NED/Fusion 2 (1985) 97 - 110

[9] D.S. Gelles and R.J. Puigh, Alloy Development for Radiation Performance, Semi-Annual Progress Report, DOE/ER/0045/11 (September 1983)

[10] J.M. Beeston, M.R. Martin, C.R. Brickman, G.E. Korth, and W.C. Francis, in Symp. on Materials Performance in Operating Nuclear Systems, Ames Laboratory, Ames, Iowa, August 1978, Nuclear Metallurgy 19, CONF-730801, pp. 59-87.

[11] J.M. Beeston et al., "Comparison of Compression Properties and Swelling of Beryllium Irradiated at Various Temperatures," EGG-FT-6608, Idaho National Engineering Laboratory (1984).

[12] R.S. Barnes and G.B. Redding, Nuclear Energy 10, p.22, 1959.

[13] J.B. Rich, G.B. Redding and R.S. Barnes, J. Nucl. Matls. 1, p. 73, 1959.

[14] L.E. Muir, Interfacial Phenomena in Metals and Alloys, Addison-Wesley Publ. Corp., Reading, MA, 1975, p. 124.

[15] W.G. Wolfer and T.J. McGarville, "Swelling of Beryllium", DAFS,

DOE/ER-0046/19, Nov. 1984.

[16] L. Yang, R. Medico, W. Baugh, and K. Schultz, "Irradiation Study of Lithium Compound Samples for Tritium Breeding Application," J. Nucl. Materials, 103, 585 (1981).

[17] Program Review Documents of the Task Force on Material and Irradiation Effects for Solid Breeders During 1980-1983, Coordinated by C.E. Johnson, ANL.

[18] A.L. Loeb, J. Amer. Ceram. Soc., 37:96 (1954).

[19] A. Biancheria, Trans. Amer. Nucl. Soc., 9:15 (1966).

[20] Y.Y. Loeb, M.C. Billone, R. Clemmer, "Solid Breeder Tritium Recovery," Blanket Comparison and Selection Study, March 20-21, 1984.

[21] "TFTR Lithium Blanket Module (LBM) Program, Preliminary Design Report," GA Technologies Report, GA-G16616, December 1981.

[22] T. Takahashi and T. Kikuchi, JAERI-M 7518 (1978).

[23] "Gel-Spere-Pac Fuel for Thermal Reactor -- Assessment of Fabrication Technology and Irradiation Performance," ORNL-5469, November 1979.

[24] M.J. Ades, "Thermal Conductivity of Sphere-Pac Fuel," Exxon Nuclear Company Report, DOE/ET/34215, July 1981.

[25] A.L. Lotts, Comp., "Fast Breeder Reactor Oxide Fuels Development -- Final Report, ORNL-49-1 (November 1973).

[26] W.D. Kingerly, "Introduction to Ceramics," John Wiley & Sons, Inc. 1967.

[27] G.W. Hollenberg, Private Conversation.